HEAT TRANSFER ANALYSIS OF THE BRIDGMAN-STOCKBARGER CONFIGURATION FOR CRYSTAL GROWTH

PART I

ANALYTICAL TREATMENT OF THE AXIAL TEMPERATURE DISTRIBUTION

by

T.J. Jasinski, W.M. Rohsenow
Department of Mechanical Engineering

and

A.F. Witt
Department of Materials Science and Engineering

Massachusetts Institute of Technology
Cambridge, Massachusetts 02139

Abstract

An analytical approach to heat transfer for crystal growth in a Bridgman-Stockbarger configuration has been developed. All first order effects on the axial temperature distribution in a solidifying charge are analyzed on the basis of a one-dimensional model whose validity could be verified through comparison with published finite difference analyses of two-dimensional models. The present model includes an insulated region between axially aligned heat pipes and considers the effects of charge diameter, charge motion, thickness and thermal conductivity of a confining crucible, thermal conductivity change at the crystal-melt interface, generation of latent heat at the interface and non-infinite charge length. Results are primarily given in analytical form and can be used without recourse to computer work for both improved furnace design and optimization of growth conditions in a given thermal configuration.

(NASA-CR-116907) HEAT TRANSFER ANALYSIS OF THE BRIDGMAN-STOCKBARGER CONFIGURATION FOR CRYSTAL GROWTH. PART 1: ANALYTICAL TREATMENT OF THE AXIAL TEMPERATURE DISTRIBUTION (Massachusetts Inst. of Tech.) G3/76

N82-27158

Unclas
23963

1. INTRODUCTION

Conventional techniques for crystal growth from the melt prove increasingly inadequate in meeting property requirements for electronic materials as dictated by advanced device technology. In this context it is of interest that renewed attention is recently being paid to seeded vertical Bridgman growth where the driving force for interfering free melt convection is reduced and the critical axial and radial thermal gradients are at least in principle readily controllable. Motivation for a thorough re-examination of this crystal growth technique is provided by ample evidence in the open literature that basic heat transfer considerations have been largely ignored in its application. These considerations are now recognized to strongly affect both crystalline and chemical perfection of the resulting solid.

In recent years several thermal analyses of Bridgman-type crystal growth systems have been reported in the literature. Noteworthy among these is a series of outstanding publications by Wilcox et al.[1,2,3] in which the effects of several dimensionless parameters on both axial and radial temperature distribution were analyzed and significant conclusions were drawn. The modeled systems, however, were simplified in several respects and the two-dimensional formulation (except for part of Chang and Wilcox[1]) precluded simple analytical results. Of interest is also the work of Davis[4] and Clyne[5,6] which demonstrates that one-dimensional models can accurately predict experimental axial temperature variations. Their models were not nondimensional and, consequently, significant thermal and geometric parameters which control the

system behavior were not identified, and their conclusions cannot readily be extended to systems of different parameter values.

The present work is part of a comprehensive integrated theoretical and experimental approach to vertical Bridgman growth in which one- and two-dimensional heat transfer models are used as a basis for optimized system design. The system (presently in construction) makes use of high temperature heat pipes which provide for axial and axi-symmetric temperature uniformity and thus for thermal boundary conditions which permit a meaningful theoretical analysis. The configuration (Fig. 1) includes, between aligned heat pipes, a gradient control region in which the crystal-melt interface is to be located. The purpose of this region, first suggested by Chang and Wilcox,[1] is to provide control of heat flow near the interface, required for the establishment of desired radial thermal gradients. The design and operation parameters are expected to provide for the system under construction a wide range of critical axial gradients and radial gradients leading to growth interface morphologies ranging from convex to concave. Primary attention is focused, however, on the establishment of growth conditions which preclude nucleation at the confining boundary with the simultaneous minimization of radial segregation effects. The use of a magnetic field for the reduction of free melt convection is provided for.

This study analyzes the effects of both system and operation parameters on the axial temperature distribution in the charge on the basis of a one-dimensional model.* This particular approach

*Radial temperature variations in the charge are the subject of a publication (Part II) presently in preparation.

was selected since oversimplified models are not required in order to provide useful and easily applied analytical results. The heat transfer analysis focuses on the following effects: geometry and material of the charge-confining crucible, diameter effect of the charge, length of the gradient control region, charge motion, thermal coupling to the furnace, charge length, generation of latent heat at the crystal-melt interface, and thermal conductivity change at the interface. Special attention is given to the axial temperature gradient at the interface and the axial position of the interface within the gradient control region.

The purpose of this analysis, which considers all first order effects on axial thermal gradients, is to provide a basis for the design of Bridgman-type growth systems and to give guidelines for optimized axial gradient control during the execution of growth experiments. Its primary asset is the timesaving element, since meaningful information can be obtained from the analytical results without resort to computer work.

2. DEVELOPMENT OF HEAT TRANSFER MODEL

The factors of concern for the development of a one-dimensional heat transfer model of the Bridgman growth system depicted in Fig. 1 are shown in Fig. 2. Hot and cold heat pipes comprise the hot and cold zones; the region between them is called the gradient zone. The length of the charge is broken down into L_H, L_G, and L_C within the hot, gradient and cold zones respectively. The charge is lowered through the furnace with a velocity V, has liquid and solid portions with different thermal conductivity, and has a

crystal-melt interface which generates latent heat. A crucible provides containment for the charge.

The model makes the following assumptions:

1. Hot and cold zone furnace temperatures are uniform, reflecting the heat pipe action, and extend to infinity in either direction.
2. The system is at all times in a quasi-steady state; i.e. transients are neglected.
3. No heat transfer by convection in the melt.
4. Heat exchange between the furnace and the charge is described by a heat transfer coefficient, h, that is constant within each zone; for simplified models in which the crucible is not taken into consideration, h is calculated between the furnace and the surface of the charge; when a crucible is included in the modeling, h is calculated between the furnace and the outer crucible surface. The gradient zone is assumed adiabatic, i.e. $h_G = 0$.
5. The one-dimensional model considers only axial heat transfer within the charge; i.e. the temperature in the charge is not a function of radius.

With these assumptions, the charge is analagous to the moving thin rod treated by Carslow and Jaeger[7] and the equation, in non-dimensional form, describing the axial temperature distribution is:

$$\frac{d^2\theta}{d\zeta^2} - Pe\,\frac{d\theta}{d\zeta} - 4Bi\theta = -4Bi\theta_f \qquad [1]$$

where:

$\zeta = z/D$ (non-dimensional axial coordinate measured from the center of the gradient zone)

$\theta = \frac{T-T_{ref}}{\Delta T_{ref}}$ (non-dimensional temperature)

θ_f = non-dimensional furnace temperature

Pe = Peclet number = VD/α

Bi = Biot number = hD/k

α = thermal diffusivity

h = heat transfer coefficient

k = thermal conductivity

V = charge displacement rate (lowering rate)

D = charge diameter

Equation [1] is applied to each region of uniform properties and Bi. In the present model there are four such regions when placing the growth interface in the gradient zone: the hot and cold zones and the liquid and solid parts of the gradient zone. Boundary conditions are equality of temperature and continuity of flux between adjacent regions. At the crystal-melt interface, the flux condition gives:

$$R_K\left(\frac{d\theta}{d\zeta}\right)_{liquid} = Pe_{solid}R_H + \left(\frac{d\theta}{d\zeta}\right)_{solid} \qquad [2]$$

where

$R_K = k_{liquid}/k_{solid}$

$R_H = \Delta H_{SL}/C_{p,solid}\Delta T_{ref}$

ΔH_{SL} = latent heat of solidification

$C_{p,solid}$ = specific heat of the solid

(The Peclet number in eq. [2] is correctly based on the actual

growth rate and it is assumed here that the growth rate is equal to the lowering rate V.)

For each region, eq. [1] yields two exponential terms for the homogeneous solution and a particular solution that depends on θ_f. The constants of integration on the exponential terms are found using the boundary conditions. This has been done analytically for systems of infinite charge length; expressions for the axial gradient in the liquid and for the temperature at the crystal-melt interface are given in the Appendix. (If the complete axial temperature distribution is required, it is more convenient to determine the constants of integration by computer.)

In consideration of the complex nature of the thermal model, a system with idealized parameter values, presently called a "symmetric" system, is used as a reference against which the effects of individual parameters will be assessed. A symmetric system is defined to have the following parameter values:

1. Equal Biot number in hot and cold zone; i.e., $Bi_H = Bi_C \equiv Bi$.
2. $Pe = 0$.
3. Equal solid and liquid thermal conductivities ($R_K = 1$).
4. No generation of latent heat ($R_H = 0$).
5. Equal charge lengths in the hot and cold zones ($L_H = L_C$).

Under such conditions, a symmetric system will have the axial temperature distribution,

$$\theta(-\zeta) + \theta(\zeta) = 1 \qquad [3]$$

3. ANALYSIS

3.1 Crucible Effect

In Bridgman growth, all charges are confined in a crucible which, depending on conditions, varies in dimension and composition. Containment of the charge tends to decrease axial gradients (Sen and Wilcox[2]). A crucible of low thermal conductivity lowers the gradient by adding thermal resistance between the charge and furnace, effectively decreasing Bi; one of high thermal conductivity lowers the gradient by "short-circuiting" heat flow within the crucible itself.

The domain of eq. [1] is here considered to be the charge only and the crucible is not explicitly included. However, a simple model of the heat transfer within the crucible allows for its consideration in eq. [1] through modified Biot and Peclet numbers.

The temperature distribution in the crucible obeys the heat conduction equation in cylindrical coordinates. Neglecting Pe effects, we obtain:

$$\frac{1}{\rho}\frac{\partial}{\partial\rho}\left(\rho\frac{\partial\theta_{cr}}{\partial\rho}\right) + \frac{\partial^2\theta_{cr}}{\partial\zeta^2} = 0 \qquad [4]$$

where:

θ_{cr} = non-dimensional crucible temperature

ρ = non-dimensional radial coordinate, r/D

r = radial coordinate

The first term of eq. [4] accounts for the radial thermal resistance of the crucible, while the second accounts for the "short-

circuit". If, at each axial location of the crucible, $\partial^2\theta_{cr}/\partial\zeta^2$ is considered to be independent of ρ and equal to $d^2\theta/d\zeta^2$ of the charge, eq. [4] can be integrated to yield a radial distribution of θ_{cr}. The boundary conditions are:

$$h_{cr}D(\theta_f - \theta_{cr}) = k_{cr}\frac{d\theta_{cr}}{d\rho} \quad \text{(at the outer crucible surface)} \qquad [5a]$$

$$\theta_{cr} = \theta \text{ (charge)} \quad \text{(at the inner crucible surface} \qquad [5b]$$

where:

h_{cr} = heat transfer coefficient between furnace and outer curcible surface

k_{cr} = thermal conductivity of the crucible

(Equation [5b] assumes that the crucible and charge are in intimate contact.) The heat flow from the crucible to the charge can thus be obtained in terms of $d\theta^2/d\zeta^2$ and used to reformulate eq. [1] through "effective" Biot and Peclet numbers:

$$Bi_{eff} = \frac{Bi_{cr}}{1 + Bi_{cr}[\frac{1}{4}(\delta^2-1) - \frac{1}{2}\ell n\delta] + K(\delta^2-1) + \frac{1}{2}\frac{1}{K}Bi_{cr}\ell n\delta} \qquad [6a]$$

$$Pe_{eff} = \frac{Pe[1 + \frac{1}{2}\frac{1}{K}Bi_{cr}\ell n\delta]}{1 + Bi_{cr}[\frac{1}{4}(\delta^2-1) - \frac{1}{2}\ell n\delta] + K(\delta^2-1) + \frac{1}{2}\frac{1}{K}Bi_{cr}\ell n\delta} \qquad [6b]$$

where:

Bi_{eff} = Biot to be used in eq. [1]

Pe_{eff} = Peclet to be used in eq. [1]

D_{cr} = outside diameter of the crucible

$$Bi_{cr} = h_{cr}D_{cr}/k$$

k = conductivity of the charge (either solid or liquid)

$\delta = D_{cr}/D$

$K = k_{cr}/k$

The relationship between the effective Biot number and the conductivity ratio K is shown in Fig. 3 for $\delta = 1.25$ and various Bi_{cr}. It can be seen that Bi_{eff} is significantly reduced by both low and high values for K. (The relationship between Bi and axial gradients will be established in Section 3.3; it shows that the present findings are in basic agreement with those of Sen and Wilcox.[2]) The conductivity ratio K which maximizes Bi_{eff} can be obtained from eq. [6]:

$$K_{(\max Bi)} = \sqrt{\frac{Bi_{cr}\ln\delta}{2(\delta^2 - 1)}} \qquad [7]$$

Taking typical values of Bi_{cr} and δ, the conductivity ratio providing for maximum axial gradients is found to lie bewteen 0.1 and 1.0. (Since all charges require confinement, the Biot and Peclet numbers used in subsequent sections are to be considered as Bi_{eff} and Pe_{eff} unless otherwise stated.)

3.2 Peclet Number Effect

Pe is the ratio of axial heat transfer in the charge due to motion and due to conduction. The effect of Pe on the axial temperature distribution in an otherwise symmetric system, obtained

through eq. [1], is shown in Fig. 4. Large Pe (e.g. high lowering rate or low thermal conductivity of the charge) increases the temperature of the charge everywhere. As a consequence, in systems with constant melting point temperature, the crystal-melt interface will move toward the cold zone; alternatively, the furnace temperatures must be lowered if the interface position is to remain fixed.

In conventional growth experiments, the Pe effect is small since the lowering rates are small (e.g. 0.1-10 μm/sec). A test criterion for its relative magnitude is provided through the characteristic roots of eq. [1]:

$$m_{\pm} = \frac{Pe}{2}\left[1 \pm \left(1 + 16\,\frac{Bi}{Pe^2}\right)^{1/2}\right] \qquad [8]$$

It can be seen that Pe disappears from eq. [8] when

$$\frac{4Bi^{1/2}}{Pe} >> 1. \qquad [9]$$

Equation [9] agrees with Chang and Wilcox[1] who reported that the Pe effect was stronger for smaller Bi. If the inequality in eq. [9] holds, the Pe effect is small enough to satisfy the Peclet number cirterion for symmetric systems (i.e. Pe ≈ 0). It should be noted (eq. [2]) that the generation of latent heat at the growth interface is also dependent on Pe. Thus, Pe has a small effect on the axial temperature distribution only if eq. [9] holds and the latent heat effect is small (see Section 3.6).

3.3 Biot Number Effect

The Biot number, through the heat transfer coefficient h, is a direct measure of the thermal coupling between the charge and the furnace. Typical values for the effective Biot number (i.e. after accounting for the crucible) vary from 0.05 for high conductivity materials such as Ge to 5.0 for low conductivity materials such as CdTe. Axial temperature profiles for several Bi, calculated from eq. [1] for symmetric systems, are shown in Fig. 5. In agreement with Chang and Wilcox,[1] it is found that the charge temperature follows more closely the furnace temperature and, as a result, the axial temperature gradient in the gradient zone increases as Bi increases.

The axial gradient behavior at the crystal-melt interface presented in the Appendix can be simplified for symmetric systems:

$$\frac{d\theta}{d\zeta} = \frac{-1}{\lambda_G + Bi^{-1/2}} \qquad [10]$$

where:

λ = non-dimensional zone length, L/D

$Bi = Bi_H = Bi_C$ for symmetric systems

$\lambda_H = \lambda_C$ = infinity

The dependence of the gradient $(d\theta/d\zeta)$ on Bi, according to eq. [10], is plotted in Fig. 6 for various gradient zone lengths (λ_G). The graphs show that the dependence of the axial gradient on the gradient zone length becomes stronger with increasing Bi. It can also

be seen (curve $\lambda_G = 0$) that there exists a minimum Bi for any desired non-dimensional axial gradient. An obvious alternative to increasing Bi for achieving larger axial gradients is to increase the temperature difference between the hot and cold zones since:

$$\frac{dT}{d\zeta} = \Delta T_{ref} \frac{d\theta}{d\zeta} \qquad [11]$$

This approach, however, is contingent on the absence of adverse side effects such as the development of excessive vapor pressures associated with increases of the hot zone temperature; it is also no viable alternative if, as a consequence of furnace temperature changes, the non-dimensional interface temperature is altered and results in the interface being shifted into an undesirable region within the gradient zone.

The Biot numbers of the hot and cold zones are generally not equal due, for example, to the temperature dependence of radiative heat transfer. For such conditions the zone with the larger Bi will more strongly influence the overall temperature level (Fig. 7). Compared to the symmetric case ($Bi_H = Bi_C$), the temperature increases everywhere within the charge when $Bi_H > Bi_C$ and decreases everywhere within the charge when $Bi_C > Bi_H$. In Fig. 7, the crystal-melt interface location for each curve is placed in the center of the gradient zone and the unequal Bi effect appears as a change in nondimensional interface temperature. To retain the interface in this location during a growth experiment necessitates a lowering of the hot and/or cold zone temperature as Bi_C decreases.

The expression for the axial temperature gradient in the gradient zone (analagous to eq. [10] for $Bi_C \neq Bi_H$) is:

$$\frac{d\theta}{d\zeta} = \frac{-1}{\lambda_G + \frac{1}{2}(Bi_C^{-1/2} + Bi_H^{-1/2})} \qquad [12]$$

where:

$\lambda_H = \lambda_C$ = infinity

System is symmetric except $Bi_C \neq Bi_H$

Interface is at the center of the gradient zone.

Equation [12] indicates that if one of the Biot numbers is much smaller than the other, it will control the axial gradient. Effort to increase axial gradients by adjusting Bi should therefore first be directed at the zone with the lower Bi.

3.4 Charge Diameter Effect

The effect of the charge diameter D on the axial temperature gradient is assessed on the basis of eq. [10]. In practice, changing D will affect other parameters as well; a corresponding change in the geometry of the furnace cavity, for example, will modify both conduction and radiation heat transfer coefficients; changes in D_{cr} and δ will also alter the effective Biot number. In order to permit isolation of the diameter effect, all other parameters are assumed fixed in the present analysis.

Since the axial coordinate in eq. [10], ζ, is non-dimensionali with respect to D, it is considered more informative to compare axial gradients based on the dimensional axial coordinate z. If

the gradient zone length, L_G, remains unchanged (i.e., λ_G varies as D^{-1}), the limiting cases for large and small Bi are given by:

$$\lim_{\substack{Bi \to \infty \\ \lambda_G \neq 0}} \left[\frac{(d\theta/dz)_2}{(d\theta/dz)_1}\right] = 1 \qquad [13a]$$

$$\lim_{Bi \to 0} \left[\frac{(d\theta/dz)_2}{(d\theta/dz)_1}\right] = \left(\frac{D_1}{D_2}\right)^{1/2} \qquad [13b]$$

where:

subscript = 1 denotes value before a change in diameter

subscript = 2 denotes value after a change in diameter

If λ_G remains unchanged (i.e., L_G varies as D), then eq. [10] gives:

$$\lim_{\substack{Bi \to \infty \\ \lambda_G \neq 0}} \left[\frac{(d\theta/dz)_1}{(d\theta/dz)_2}\right] = \frac{D_1}{D_2} \qquad [14a]$$

$$\lim_{Bi \to 0} \left[\frac{(d\theta/dz)_2}{(d\theta/dz)_1}\right] = \left(\frac{D_1}{D_2}\right)^{1/2} \qquad [14b]$$

The relationship between the axial gradient and changes in D as a function of the initial Biot number, Bi_1, (i.e., Bi based on the initial system with charge diameter D_1), is presented in Fig. 8. Accordingly, increasing the charge diameter (D) will decrease the dimensional axial gradient unless compensated for by other changes. The effect of decreasing the charge diameter, on the other hand, is a function of Bi. For large Bi a decrease in D will produce a large increase in axial gradient if associated with a simultaneous decrease in λ_G. If Bi is small, regardless of the magnitude of λ_G,

any decrease in D will enhance the axial gradient, however, to a lesser extent than with a large Bi.

3.5 Thermal Conductivity Change at the Crystal-Melt Interface

The effect of R_K on the axial temperature distribution according to eq. [1] is shown in Fig. 9 for systems which are otherwise symmetric (i.e., $Bi_H = Bi_C/R_K$). In all instances, the charge phase with higher thermal conductivity exhibits a lower axial gradient because of lower thermal resistance to heat transfer in the axial direction. For charges with $R_K > 1$, the axial gradient in the melt near the interface is therefore less than in the solid. The functional relationship between the axial gradient in the melt at the melt-crystal interface and R_K, analagous to eq. [10], is:

$$\left(\frac{d\theta}{d\zeta}\right)_{\substack{\text{in melt at}\\ \text{interface}}} = \frac{-2}{Bi_C^{-1/2}(R_K + R_K^{1/2}) + \lambda_G(R_K + 1)} \qquad [15]$$

where:

$Bi_H = Bi_C/R_K$

$\lambda_H = \lambda_C =$ infinity

$R_K \neq 1$; system is otherwise symmetric

Interface is at the center of the gradient zone

Comparing eqs. [15] and [10], it is seen that, independent of Bi, any increase in R_K results in a decrease of the axial gradient in the melt. The axial gradient as a function of R_K according to eq. [15] is plotted in Fig. 10 for several Bi_C values with $\lambda_G = 1.0$. Applying eq. [15] to germanium ($R_K \approx 2.5$), for example, it is found

that the conductivity effect reduces the interfacial melt gradient by about 50%.

3.6 Latent Heat Effect

The generation of latent heat of solidification at the melt-crystal interface enters the solution of eq. [1] only through the boundary condition at this interface (eq. [2]). (Pe in this section is not Pe_{eff}, but should be interpreted as defined in eq. [1].) For the symmetric case ($R_K = 1$), the axial temperature gradient in the liquid at the crystal-melt interface thus becomes:

$$\frac{d\theta}{d\zeta} = \frac{-2 + Pe_S R_H (Bi^{-1/2} + \lambda_G)}{2(Bi^{-1/2} + \lambda_G)} \qquad [16]$$

where:

$Bi = Bi_C = Bi_H$

$\lambda_H = \lambda_C =$ infinity

$Pe_S R_H \neq 0$; system is otherwise symmetric

Interface is at the center of the gradient zone

For $R_K \neq 1$, the axial gradient assumes the form:

$$\frac{d\theta}{d\zeta} = \frac{-2 + Pe_S R_H (Bi_C^{-1/2} + \lambda_G)}{Bi_C^{-1/2}(R_K + R_K^{1/2}) + \lambda_G(1 + R_K)} \qquad [16a]$$

where:

$Bi_H = Bi_C / R_K$

From eq. [16] is can be seen that the effect of the latent heat on axial gradients (and also on the temperature profile) will be small if:

$$\frac{1}{2}(Pe_S R_H)(Bi^{-1/2} + \lambda_G) \equiv \phi << 1 \qquad [17]$$

Equation [17] demonstrates that the effect of latent heat on the axial temperature behavior increases as Bi decreases.

Axial temperature profiles calculated from eq. [1] for various values of ϕ are plotted in Fig. 11 where, in order to isolate the latent heat effect, Pe was chosen small enough so that eq. [9] is satisfied. It can be seen that the generation of latent heat both increases the charge temperature and decreases the axial gradient at the interface in the melt. For small values of ϕ, the latent heat effect disappears and the axial temperature profile approaches that of symmetric systems.

3.7 "Infinite" Charge Length

The contribution from the positive characteristic root, eq. [8], to the solution of eq. [1] is normally small and is zero for an infinite charge length. The charge thus appears infinite in length when the contribution from the negative root also becomes small, i.e., for large ζ. The temperature change within the hot or cold zone reaches approximately 99% of its final value when $\exp[(m_-)\zeta] = 0.01$. Using this as a criterion for infinite length:

$$\zeta_\infty \gtrsim \frac{5}{m_-} \qquad [18]$$

where:

ζ_∞ = length of charge in hot or cold zone for charge to appear infinitely long

If Pe is small so that eq. [9] is satisfied, the characteristic roots become:

$$m_\pm = \pm 2\sqrt{Bi} \qquad [19]$$

and by substitution we find:

$$\zeta_\infty \geq \frac{5}{2\sqrt{Bi}} \qquad [20]$$

which is a useful expression for determining ζ_∞.

For any charge length which appears infinite in both the hot and cold zones, the temperature field of the charge will not change (interface position remains fixed) as it is lowered through the gradient zone. Figure 12 shows the progression of axial temperature profiles as the charge moves from the hot zone to the cold zone for charge lengths less than infinite. It can be seen that charge temperatures are displaced toward the hot zone furnace temperature when most of the charge is in the hot zone and vice-versa. Accordingly, to achieve constant interface position for non-infinite charge lengths, the nondimensional melt temperature must be reduced as the experiment proceeds. At constant nondimensional melt temperature, the interface will move from the cold zone toward the hot zone and the interface growth velocity will be greater than the lowering rate. This finding is in agreement with the experimental results of Clyne[5,6] which suggest that longer charges and higher Bi will tend to stabilize the interface position (growth rate is

the same as the displacement rate).

When the charge length is not "infinite", appropriate boundary conditions must be applied to the ends of the charge. For a solid pull rod, an approximate Bi can, for example, be obtained by treating it as a simple fin, exchanging heat with the environment. The curves of Fig. 12 were calculated using for the ends the same Bi as for the circumference.

3.8 Effect of Radial Gradients on the Axial Temperature Profile

In the development of eq. [1], the radial temperature distribution of θ at each axial location ζ was considered constant. Presently, radial gradients in the charge are considered insofar as they affect the preceding results for the axial temperature distribution.

The heat transfer between the furnace and charge accounted for in the Bi term of eq. [1] depends on the temperature difference between the furnace wall and the charge surface. This temperature difference can be accommodated in eq. [1])

$$\frac{d^2\theta}{d\zeta^2} - Pe \frac{d\theta}{d\zeta} = -4Bi(\theta_f - \theta_s) \qquad [21]$$

where:

θ_s = surface temperature of charge

Integrating each term of eq. [21] with respect to the cross sectional area of the charge and assuming that the average of the derivatives

is approximately equal to the derivative of the averages, we find:

$$\frac{d^2\overline{\theta}}{d\zeta^2} - Pe\,\frac{d\overline{\theta}}{d\zeta} = -4Bi[(\theta_f - \overline{\theta}) - (\theta_s - \overline{\theta})] \qquad [22]$$

where:

$$\overline{X} \equiv \int_{area} X \cdot d(area)$$

[In eq. [22] the radial gradients are expressed by the term $(\theta_s - \overline{\theta})$.] If the radial temperature distribution within the charge is approximated as was done for the crucible in Section 3.1, we obtain:

$$(\theta_s - \overline{\theta}) \simeq \frac{-1}{32}\,\frac{d^2\overline{\theta}}{d\zeta^2} \qquad [23]$$

Combining eq. [23] with eq. [22] leads to a relationship for an effective Bi, (Bi^*_{eff}), which accounts for radial temperature gradients within the charge:

$$Bi^*_{eff} = \frac{Bi}{1 + \frac{Bi}{8}} \qquad [24]$$

where:

Bi = Biot as defined in Section 3.1 (accounting for crucible effect, but not for radial gradient effect)

Bi^*_{eff} = Biot accounting for both crucible effect and radial temperature gradients in the charge

Equation [24] can be used to approximate the effect of radial gradients on the axial temperature distribution if Bi/8 is not small compared to unity. If Bi/8 is small compared to unity, on the other

hand, eq. [1] reasonably predicts the axial temperature profile.

The validity of eq. [24] can be tested on the basis of data obtained through the two-dimensional finite difference model by Fu and Wilcox.[3] Figure 3 of their paper presents the radial variation of the axial gradient at the interface of symmetric systems for several Bi and λ_G. Point values from these curves were numerically integrated to obtain the average axial gradient over the cross section and were compared to the values obtained using eqs. [10] and [24] (see Table 1). Considering the approximations required in the derivation of eq. [24], the agreement of the data must be taken as excellent. The comparison demonstrates that the one-dimensional models presently used provide a meaningful representation of the parameters governing the axial temperature behavior of charges in a Bridgman-type growth configuration.

4. DISCUSSION AND CONCLUSIONS

The one-dimensional model developed in Section 2 has been shown to correlate well with a corresponding two-dimensional model of Sen and Wilcox[2] concerning the axial temperature distribution in a solidifying charge. It is expected, therefore, that the results derived from this model accurately demonstrate the effects of furnace and material property parameters and can be applied to the optimization of both furnace design and execution of growth experiments. The model is easily applied to machine computation. Its primary asset, however, lies in the fact that it yields extremely useful and relatively simple analytical relationships. For example, criteria could thus be derived which define the conditions under which

the effects of charge motion, length of charge in the hot and cold furnaces, and the generation of latent heat can be neglected; the effects of thickness and thermal conductivity of a confining crucible could be accounted for by a simple modification of the Bi parameter.

The model indicates that the axial gradient in the liquid at the interface is adversely affected (decreases) by the following charge properties:

- Large thermal conductivity
- Large latent heat of solidification
- Large R_K (k_{liquid}/k_{solid})

Maximization of axial gradients in the charge can be approached through several operational and design options, each of which, however, has its limitations and potential drawbacks:

Biot Number: Axial thermal gradients can be increased by increasing the heat transfer coefficients (h) in both the hot and the cold zones (eq. [10]). Since in typical high temperature growth experiments heat transfer is largely controlled by radiation, it is imperative that furnace emissivities be kept high. (Within the gradient zone, however, undesirable radial heat transfer can be reduced through the installation of highly reflecting radiation shields.) Given the third power temperature dependence of the radiation heat transfer coefficient, an increase of the furnace temperature will also increase Bi. This approach, however, has its limitations in systems which develop high vapor pressures and thus require special crucible materials and construction, which in turn may reduce Bi.

Heat conduction across the gap between the furnace and the crucible can significantly contribute to the overall heat transfer coefficient if the gap width is small and the gas has a high thermal conductivity. For example, He in a one millimeter gap will transfer about the same quantity of heat by conduction as is transferred by radiation at 900°C. Small gap widths, however, accentuate errors in centering the charge within the furance cavity and thus will prevent the establishment of axi-symmetric boundary conditions.

Gradient Zone Length: For any given temperature difference between the hot and cold zones, a decrease in the gradient zone length, λ_G, will increase the axial gradient, especially for large Bi (eq. [10]). A smaller λ_G, however, will also produce larger radial gradients in the gradient zone,[3] and the precision with which the interface must be localized in order to satisfy radial gradient criteria will increase.

Charge Diameter: For a given system, any decrease in charge diameter will decrease Bi and thus the nondimensional axial gradient, but will increase the dimensional axial gradient (see Section 3.4). This effect is most pronounced for large Bi and when accompanied by a decrease in λ_G.

Furnace Temperature Difference Between Hot and Cold Zones: Increasing ΔT_{ref} will produce a proportional increase in the axial gradient, eq. [11].

Crucible: To prevent a severe reduction in Bi_{eff}, the thermal conductivity of the crucible should be close to that of the charge. In systems with large conductivity differences between the liquid and solid charge, the conductivity of the crucible should be chosen

so that the nondimensional axial gradient is maximized according to eq. [12]. A thin crucible (δ close to unity) also serves to keep Bi_{eff} high. If vapor pressure considerations are important, the resultant decrease in crucible strength can be overcome by pressurizing the furnace system. An alternate approach to maximizing Bi_{eff} consists of the use of coated metallic crucibles.

Growth Rate: If the generation of latent heat is significant (eq. [17]), a decrease in the growth rate (smaller $Pe_S R_H$) will serve to increase the axial gradient in the liquid at the interface.

The present study of functional relationships concerning the axial temperature distribution in Bridgman configurations is of obvious importance for gradient control and the related morphological stability of the growth interface. Moreover, axial gradient control is interrelated to the nucleation and segregation affecting radial thermal gradient control, dealt with in Part II of this work.

ACKNOWLEDGMENTS

The authors wish to express their appreciation to the National Aeronautics and Space Administration (Materials Processing in Space Division, Grant No. NSG 7645) for their financial support and cooperation in this study.

REFERENCES

1. Chang, C.E., and Wilcox, W.R., J. Crystal Growth 21, 135 (1974).
2. Sen, S., and Wilcox, W.R., J. Crystal Growth 28, 36 (1975).
3. Fu, T.-W., and Wilcox, W.R., J. Crystal Growth 48, 416 (1980).

4. Davis, K.G., Can. Met. Quart. 11 (2) 317 (1972).

5. Clyne, T.W., J. Crystal Growth 50, 684 (1980).

6. Clyne, T.W., J. Crystal Growth 50, 691 (1980).

7. Carslaw, H.S., and Jaeger, J.C., Conduction of Heat of Solids, 1st ed., Oxford University Press, Amen House, London, p. 128 (1947).

APPENDIX

For an infinite charge length and crystal-melt interface position within the gradient zone, the model of Section 2 yields the following expression for the axial gradient in the liquid at the interface:

$$\frac{d\theta}{d\zeta} = \frac{\dfrac{m_4}{1 + \left(\dfrac{m_4}{m_2} - 1\right) e^{m_4(\mu - \zeta_m)}} + Pe_S R_H}{R_K - \dfrac{m_4}{m_3} \dfrac{\left[1 + \left(\dfrac{m_3}{m_1} - 1\right) e^{-m_3(\mu + \zeta_m)}\right]}{\left[1 + \left(\dfrac{m_4}{m_2} - 1\right) e^{m_4(\mu - \zeta_m)}\right]}}$$

where:

$$m_1 = \frac{Pe_L}{2}\left[1 + \left(1 + 16\,\frac{Bi_H}{Pe_L^2}\right)^{1/2}\right]$$

$$m_2 = \frac{Pe_S}{2}\left[1 - \left(1 + 16\,\frac{Bi_C}{Pe^2}\right)^{1/2}\right]$$

$$m_3 = Pe_L$$

$$m_4 = Pe_S$$

Pe_L = Peclet number based on liquid properties

Pe_S = Peclet number based on solid properties

Bi_H = Biot number in hot zone (based on liquid properties)

Bi_C = Biot number in cold zone (based on solid properties)

$$\mu = \frac{1}{2}(L_G/D) = \frac{1}{2}\lambda_G$$

ζ_m = dimensionless interface position with respect to the center of the gradient zone. $-\mu < \zeta_m < +\mu$.

The relation between interface temperature (θ_m) and position (ζ_m) is given by:

$$1 - \theta_m = \frac{\dfrac{m_4}{1 + \left(\dfrac{m_4}{m_2} - 1\right) e^{m_4(\mu - \zeta_m)}} + Pe_S R_H}{\dfrac{m_4}{1 + \left(\dfrac{m_4}{m_2} - 1\right) e^{m_4(\mu - \zeta_m)}} - \dfrac{R_K m_3}{1 + \left(\dfrac{m_3}{m_1} - 1\right) e^{-m_3(\mu + \zeta_m)}}}$$

Note that an iterative solution is required if it is desired to determine ζ_m given θ_m.

For a symmetric system, eq. [9] holds and m_1 and m_2 can be approximated by eq. [20]. This leads to a simplified form of the axial gradient expression, which is used in Section 3.

Table 1. Axial thermal gradients at the crystal-melt interface as obtained through eqs. [10] and [24], $d\bar{\theta}/d\zeta$, and average axial thermal gradients $(d\theta/d\zeta)_{av}$, as determined from the two-dimensional model of Fu and Wilcox.[3]

		$\left(\frac{d\theta}{d\zeta}\right)_{av}$ Fu and Wilcox[3]	$\frac{d\bar{\theta}}{d\zeta}$ Eqs. [10] and [24]
Bi = 2	$\lambda_G = 0$	1.310	1.260
	$\lambda_G = 0.25$	0.975	0.961
	$\lambda_G = 0.50$	0.778	0.775
Bi = 0.4	$\lambda_G = 0$	0.616	0.617
	$\lambda_G = 0.5$	0.464	0.472

•symmetric system
•infinite ends

FIGURE CAPTIONS

Fig. 1 Modified Bridgman-Stockbarger configuration.

Fig. 2 Thermal model of furnace and charge with crucible.

Fig. 3 Effect of thermal conductivity of a crucible on the effective Biot number.

Fig. 4 Effect of charge motion on the axial temperature distribution in a charge.

Fig. 5 Effect of thermal coupling between furnace and charge on the axial temperature distribution within the charge.

Fig. 6 Effect of gradient zone length and Bi on the axial temperature gradient in the melt at the crystal-melt interface.

Fig. 7 Effect of unequal hot and cold zone Bi on the axial temperature distribution in the charge.

Fig. 8 Effect of charge diameter on the axial temperature gradient at the crystal-melt interface. (The axial coordinate is dimensional.)

Fig. 9 Effect of difference in thermal conductivity of crystal and melt on the axial temperature distribution in the charge.

Fig. 10 Effect of thermal conductivity ratio (R_K) and Bi on the axial temperature gradient in the melt at the crystal-melt interface.

Fig. 11 Effect of the generation of latent heat at the growth interface on the axial temperature distribution in the charge.

Fig. 12 Effect of charge position within the furnace on the axial temperature distribution.

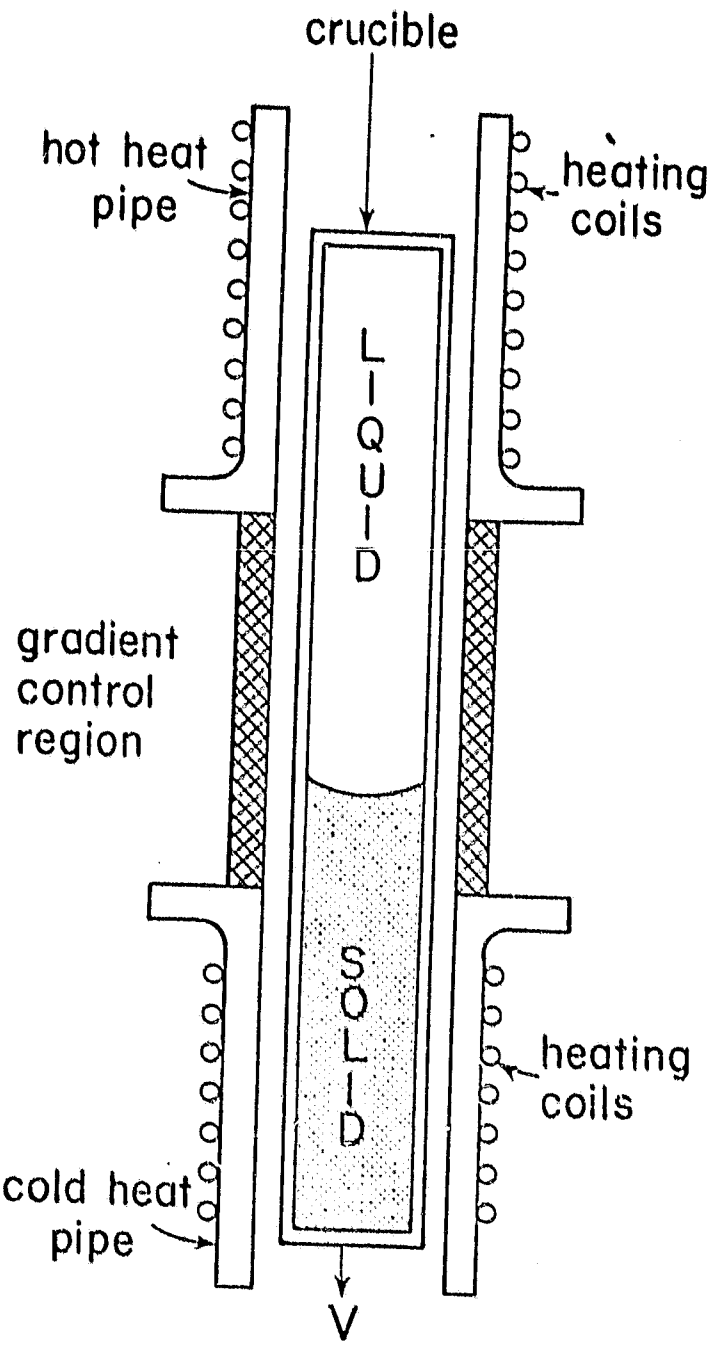

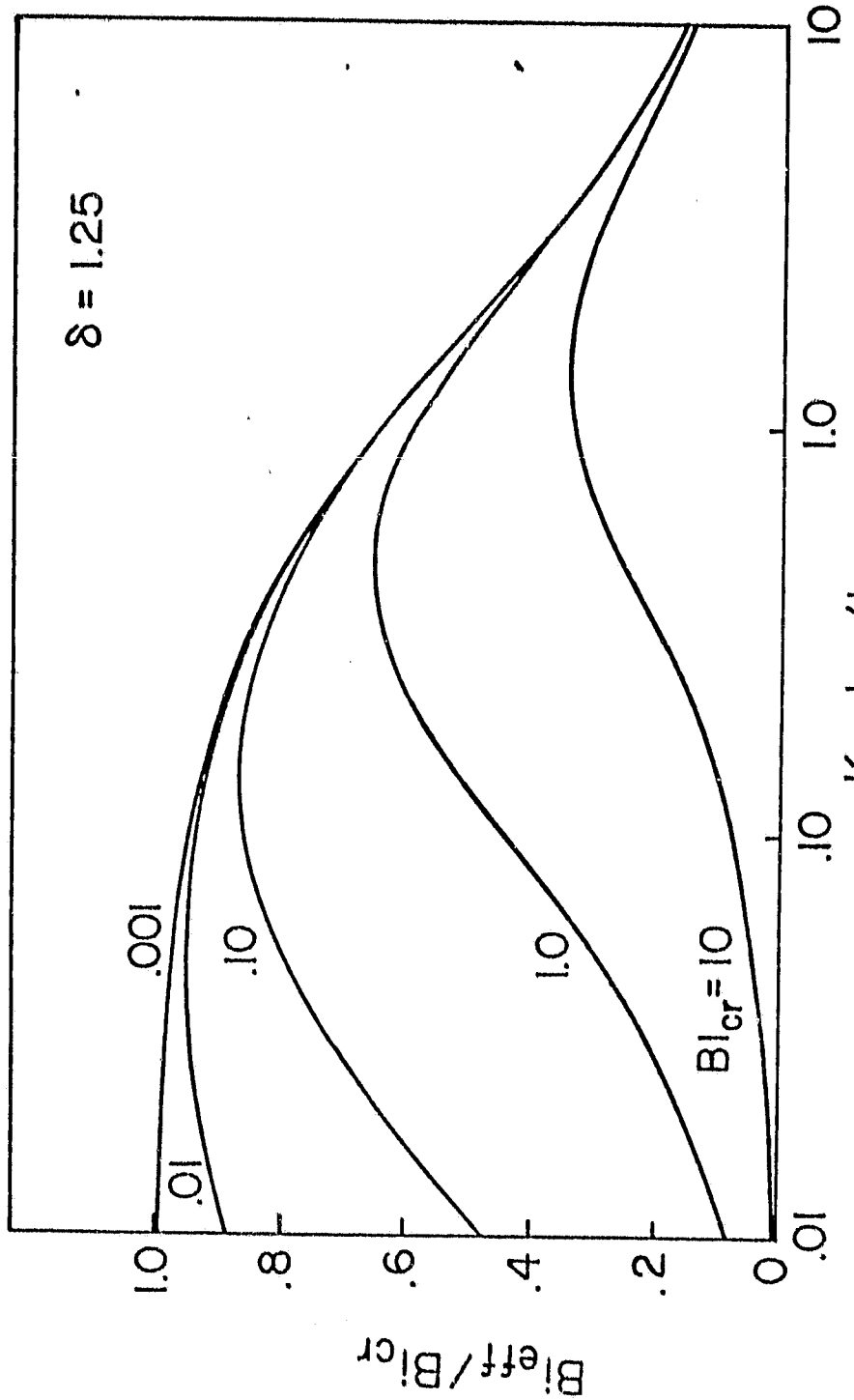

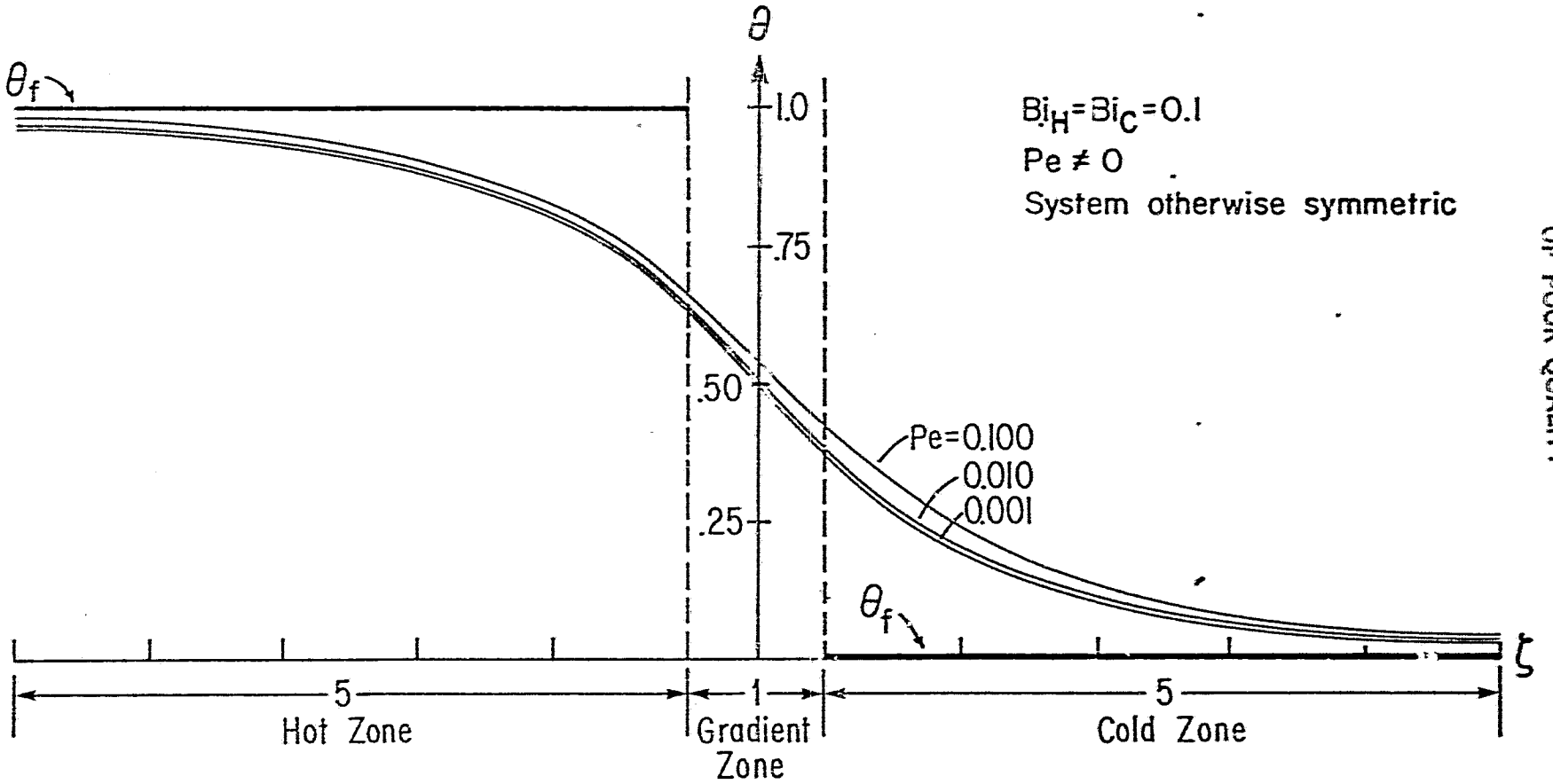

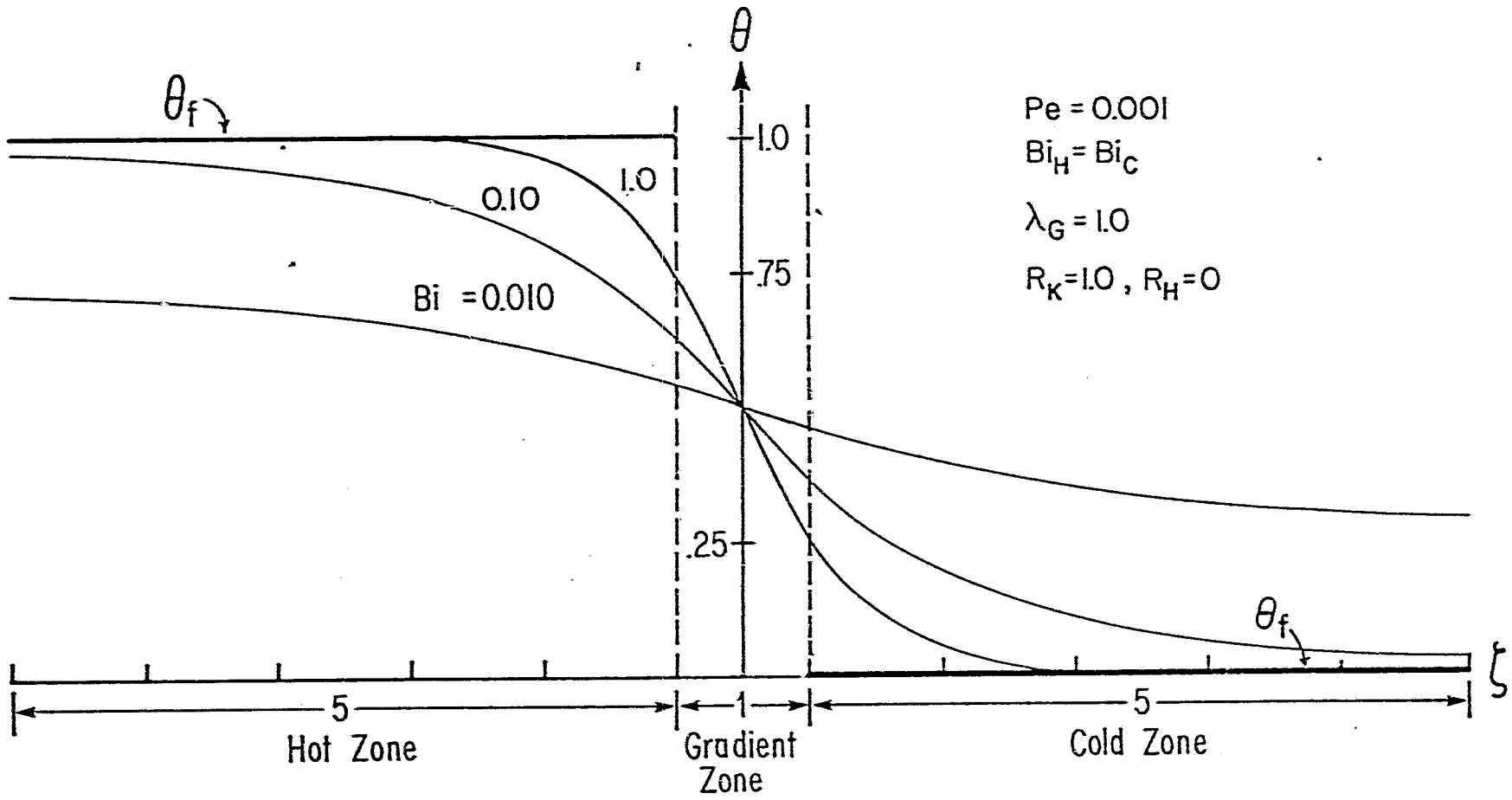

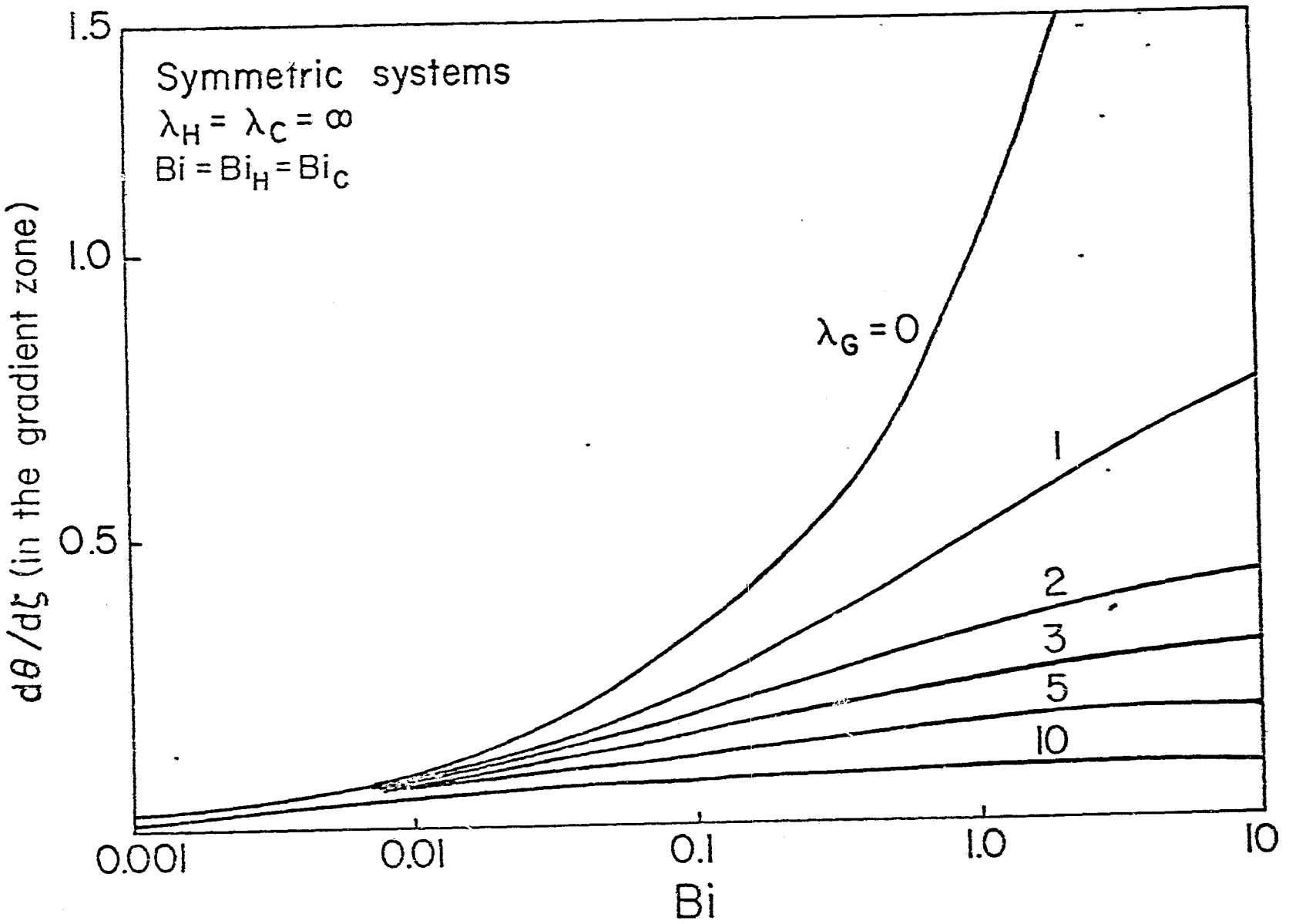
Symmetric systems
$\lambda_H = \lambda_C = \infty$
$Bi = Bi_H = Bi_C$
$\lambda_G = 0$
1
2
3
5
10
1.5
1.0
0.5
$d\theta/d\zeta$ (in the gradient zone)
0.001
0.01
0.1
1.0
10
Bi